KRONOS FUSION ENERGY

PAPER 2.22 · THE KRONOS 2026 SERIES

Vacuum-Vessel and Support Structural Mechanics Under Electromagnetic, Halo-Current, and Seismic Loads for a Compact Spherical-Tokamak Breeder

The vacuum vessel and its support carry the entire electromagnetic, thermal and inertial load path of a compact spherical-tokamak breeder into the ground, and in a...

Read it live — 3-D model · physics validator · film series

BY P I FORDOFFICIAL VERSION: KRONOSFUSIONENERGY.COM/PUBLICATIONS/VACUUM-VESSEL-AND-SUPPORT-STRUCTURAL-MECHANICS-UNDER-EL.HTML, R J WEGGEL AND C WEGGEL

2026 · EDITORIAL EDITION

THE OFFICIAL RECORD

What this document is, and how to read its numbers

This is a combined editorial. It gathers, in one volume, the two design studies Kronos Fusion Energy released in 2026 — a compact spherical-tokamak tritium/helium-3 breeder and a deuterium–helium-3 tandem-mirror generator — together with the intellectual-property estate, the people, and, in the internal edition, the full commercial case. The scientific text is the same text that appears in the arXiv preprints and the journal submissions; the editorial adds the apparatus a reader needs to hold the whole program at once, and nothing in the physics is altered to fit it.

THE HONESTY STANCE IS THE ASSET

Every headline quantity carries an **evidence class** — DERIVED RECOMPUTED MEASURED REQUIREMENT — and, where a number is a modelled extrapolation rather than a demonstrated value, it is labelled as such and its downside is shown next to it. Several quantities in the underlying corpus moved after first publication; where a value has been withdrawn or restated, the record says so plainly. This is deliberate: a diligence team will find the load-bearing assumptions, so the document surfaces them first.

TWO EDITIONS

This volume is issued in two editions. The **public edition** (light) carries the physics and the design only — no dollar, price, or per-kilogram figure appears anywhere in it. The **internal edition** (dark) adds the economics, the funding architecture, and the defense-commercial analysis, and is marked *Confidential* accordingly; it is not for public distribution. Where the commercial case rests on a modelled assumption rather than a demonstrated one, it is labelled as such and its downside is shown alongside it, on the same terms as the physics.

TITLE	The Kronos Fleet — Hyperion · Aegis · MetroVolt: A Combined Design & Commercialization Study
AUTHOR	Priyanca Ford, Founder & CEO, on behalf of Kronos Fusion Energy
EDITION	2026 Combined Editorial · first issue
COMPANION WORKS	The five-paper arXiv drop — (1) Breeder, (2) Burner, (3) REBCO magnet & tape, (4) Direct Energy Conversion, (5) AI/ML/Quantum control — with matching numbered Zenodo deposits, plus the IOP journal and IAEA-FEC submissions. Patents were filed before the drop.
NAMING	Hyperion = the breeder; Aegis (defense) and MetroVolt (data-center) = one generator in two housings. Internal mode letters (D1, L) do not appear on public surfaces.
STATUS	Conceptual design & simulation study. Nothing herein is a construction commitment.

HOW TO READ THIS VOLUME

The fleet at a glance, and the way its numbers are marked

This volume opens with *Orientation*, presents the five research papers as a bound sequence, and closes with the *Apparatus*. *Foundations* sets out the three general results both machines rest on. *Paper One* is the Hyperion breeder; *Paper Two* the Aegis / MetroVolt generator; *Papers Three, Four and Five* are the enabling science — high-field REBCO magnets and tape, direct energy conversion, and the AI / ML / quantum control stack. A *Digital Twin & 3-D Model* part follows, then the *Environmental* profile. The *Economics* and levelized cost and the *Business Case* and diligence record appear in the internal edition only; the *Simulations* proof record and the Apparatus — patent portfolio, team, limitations, and sources — close both editions.

THE FLEET AT A GLANCE

	HYPERION	AEGIS	METROVOLT
Role	Strategic-isotope foundry	Defense installation power	Campus power
Machine	**Spherical tokamak**	**Tandem mirror**	**Tandem mirror**
Fuel	Deuterium–tritium	Deuterium–helium-3	Deuterium–helium-3
Delivers	Tritium · ^{3}He · 14 MeV n	Resilient installation power	Firm campus power
Physics bar	**Fusion gain only**	Closure (gates named)	Closure + lunar ^{3}He
In the fleet	Breeds the fuel	Proves the generator	Commercial destination

HOW THE NUMBERS ARE MARKED

Every headline quantity carries an evidence class — DERIVED from first principles, RECOMPUTED from raw data, MEASURED in hardware, or a REQUIREMENT yet to be met. Financial figures carry a case label and are confined to the internal (confidential) edition. Values that moved after first publication are shown as withdrawn or restated rather than quietly changed. A capability you can evaluate is one whose limits are on the page.

ABSTRACT

Vacuum-Vessel and Support Structural Mechanics Under Electromagnetic, Halo-Current, and Seismic Loads for a Compact Spherical-Tokamak Breeder

The vacuum vessel and its support carry the entire electromagnetic, thermal and inertial load path of a compact spherical-tokamak breeder into the ground, and in a high-power-density device the impulsive disruption load, not the steady field or the seismic base excitation, sets the design. We formalise the vessel-and-support structural-mechanics problem for the Hyperion breeder (design point $I_p = 9.66\,MA$, $Q = 3.076$, $P_{\text{fus}} = 85.04\,MW$, negative triangularity $\delta = -0.30$, $B_0 = 8\,T$, elongation $\kappa = 2.0$, major radius $R_0 = 1.20\,m$, aspect ratio $A = 2.5$, centrepost peak field $16.84\,T$) as a coupled thermo-electro-mechanical continuum problem, and we solve it load case by load case with retained margin. We write the governing momentum balance, the Maxwell-stress electromagnetic body force, the thermoelastic constitutive law, the halo-current and eddy force integrals, the modal response-spectrum seismic formulation, and the linear-elastic-fracture-mechanics flaw criterion as explicit equations, and we cast the qualification as a ladder of inequalities against the 800 MPa structural allowable. Under the electromagnetic self-load the $16.84\,T$ field produces a $113\,MPa$ magnetic pressure and a near-hydrostatic $-190\,MPa$ compression that holds the equivalent von Mises stress to $84\,MPa$; a combined cooldown-plus-quench-plus-electromagnetic transient with fast quench detection caps the hot-spot at 63 K and the combined von Mises at **245 MPa** ($3.3\times$), so detection speed *is* structural margin; the highest-fidelity finite-element model on the real centrepost CAD keeps the structural jacket to $579\,MPa$ ($1.38\times$) and the conductor hoop strain to 0.151% ($2.65\times$), and an engineered per-turn precompression winding cuts the peak REBCO hoop strain by 52.4% and flattens its profile $4.8\times$. The disruption halo/eddy envelope — halo current $\approx 2.9\,MA$, vertical force $\approx 23\,MN$ over a 7–$19\,ms$ current quench — dominates the support design, standing two orders of magnitude above a design-basis seismic base shear of $\approx 0.2\,MN$; the cryogenic 316LN jacket is leak-before-break, with a critical flaw of 333 mm at operating stress against a 2 mm inspection threshold and a Paris-law fatigue life of order 10^8 cycles. Every result is grounded in the Kronos Physics De-Risking Register and was produced on a GPU-accelerated finite-element campaign. The binding constraint on the structure is neutron lifetime, not stress; the burner plug coil at $26.49\,T$ is a distinct magnet, analysed separately.

Open-access deposit (code & data, CC BY 4.0): DOI 10.5281/zenodo.22645838 · Zenodo community *kronos_fusion_energy*. Explore it live: interactive 3-D model · physics validator.

Keywords: structural mechanics · vacuum vessel · disruption halo current · seismic response spectrum · leak-before-break · REBCO magnet · spherical-tokamak breeder

CONTENTS

Table of Contents

NOMENCLATURE

Symbols, units, and the names of things

Q	plasma (fusion) gain, P_{fus}/P_{aux}
Q_E	engineering gain, net electric out / recirculating in
H_{98}	confinement enhancement over the IPB98(y,2) scaling
Z_{eff}	effective ion charge
c_{ee}	electron–electron bremsstrahlung leading coefficient, 2.120022 (exact)
τ_E	energy confinement time
I_p	plasma current
R_0, a	major radius, minor radius
κ, δ	elongation, triangularity
β_N	normalized plasma beta (Troyon-normalized)
TBR	tritium breeding ratio
DEC	direct energy conversion
CF	plant capacity factor (availability)
FOAK / NOAK / BOAK	first / n^{th} / best of a kind
Hyperion	the ST breeder (internal: Mode D2)
Aegis	the generator, defense/installation housing (internal: Mode M)
MetroVolt	the generator, data-center housing (Mode M)

structural mechanics; vacuum vessel; disruption halo current; seismic response spectrum; leak-before-break; REBCO magnet; spherical-tokamak breeder

§ 1

Introduction

THE STRUCTURAL PROBLEM OF A COMPACT SPHERICAL-TOKAMAK BREEDER

A spherical tokamak (ST) confines a large plasma current in a small volume, which is what makes it an attractive neutron source and breeder platform [1,2] and, at the same time, what concentrates its mechanical loads. The Hyperion breeder holds $I_p = 9.66\,MA$ at a major radius of only $R_0 = 1.20\,m$ behind a centrepost magnet at a peak field of $16.84\,T$, in a negative-triangularity ($\delta = -0.30$) regime that accesses good confinement without the edge pressure pedestal and the associated edge-localised-mode cycle of conventional H-mode [3,4]. The vacuum vessel is the pressure and vacuum boundary, the first structural ring outside the plasma, and the member that carries every load the machine generates — the steady electromagnetic self-load of the magnets, the thermal excursions of cooldown and of a quench, the impulsive forces of a plasma disruption, and the seismic base excitation of the site — into the support and the ground, while a 14 MeV neutron flux slowly consumes the material of the innermost members.

Three features make this problem distinct from that of a conventional aspect-ratio tokamak. First, the compactness that gives the ST its high power density leaves little radial room for structure precisely where the field and the current density are highest, so the vessel and its support cannot be sized by strength margin alone — they must be reconciled with a tight radial budget. Second, the high plasma current in a small volume makes the disruption the governing mechanical event: at $I_p = 9.66\,MA$ a vertical displacement event drives halo currents of mega-ampere scale through the vessel and the support in milliseconds, and the resulting Lorentz forces dwarf the steady loads. Third, the small seismic mass of a compact machine makes the seismic base shear small in absolute terms, so that the seismic case — which sizes the support of a large light-water reactor — is here a subdominant check rather than the governing load. Quantifying that hierarchy, and closing every load case against a single allowable, is the purpose of this paper. Figure 1 orients the load path: the electromagnetic self-load, the disruption halo force, and the seismic base excitation all resolve through the vacuum vessel and the bucked-and-wedged support into the ground.

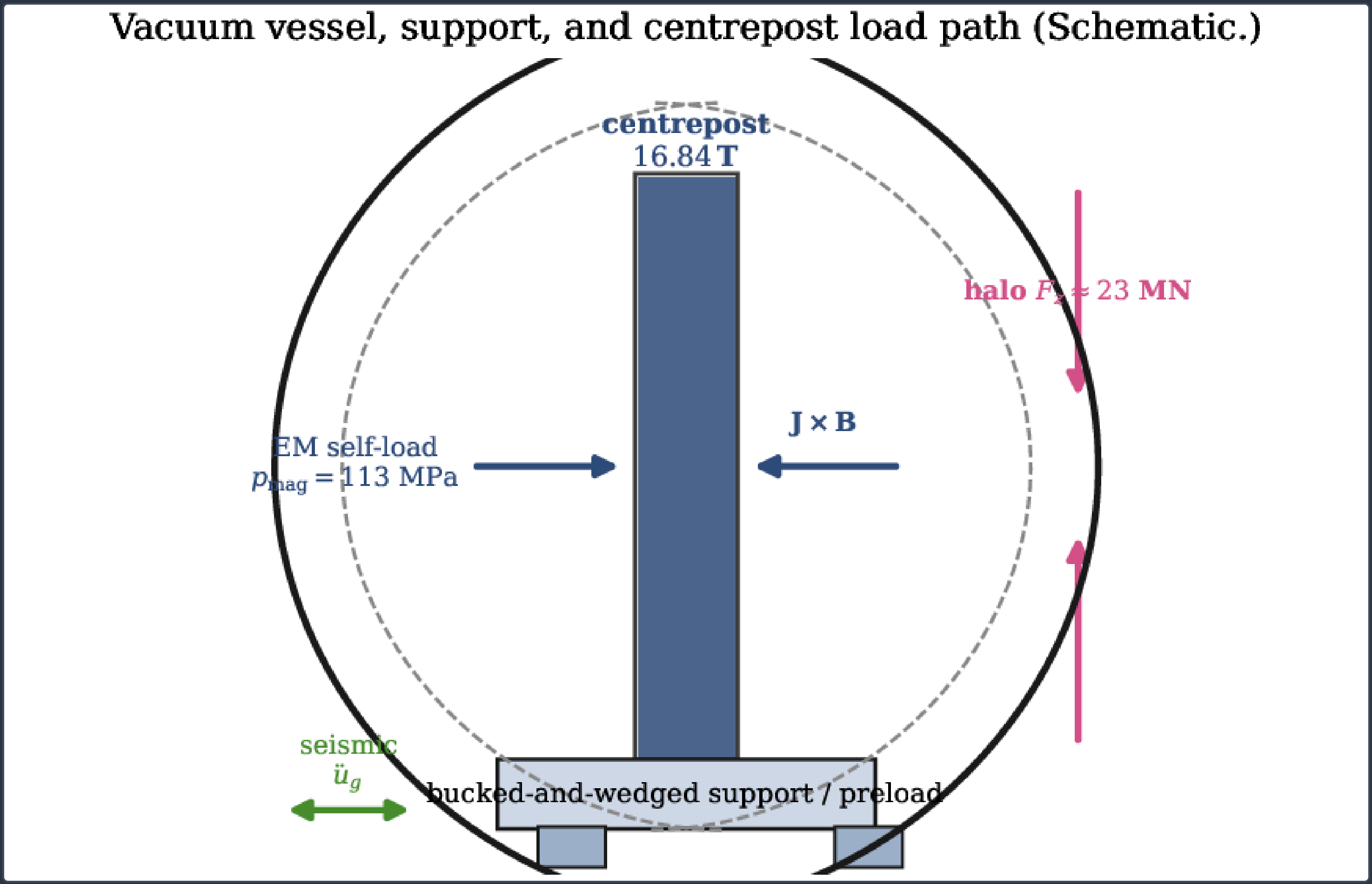

(Schematic.) The vacuum vessel, bucked-and-wedged support, and $16.84\,T$ centrepost, and the three load classes they carry: the electromagnetic self-load $J \times B$, the disruption halo vertical force $F_z \approx 23\,MN$, and the seismic base excitation $\ddot{u}_g$. The figure encodes the load path only; no data values are plotted.

PRIOR ART

Tokamak vessel and support structural mechanics is a mature engineering discipline. The ITER vacuum vessel is a double-walled, code-qualified structure whose design and construction have been documented in detail [5], and the disruption electromagnetic-load basis for large tokamaks is codified in the ITER Physics Basis [6] and in the disruption-mitigation strategy that follows from it [7,8]. Halo currents — the poloidal currents that flow through the plasma scrape-off layer and close through the conducting vessel during a vertical displacement event — have been characterised experimentally, notably on the National Spherical Torus Experiment, where their toroidal asymmetry and rotation set the local force peaking [9], and the vertical forces they generate in an ITER-scale plasma have been quantified with three-dimensional magneto-hydrodynamic modelling [10]. The eddy-current and passive-conductor problem that accompanies the halo load is now addressed with dedicated thin-wall electromagnetic codes [11]. On the magnet side, the structural design of a spherical-tokamak centre stack under combined electromagnetic, thermal and structural loading was worked out in detail for the NSTX-Upgrade ohmic-heating coil and centre stack [12], and the cryogenic structural materials that carry these loads — austenitic stainless steels at 4 K — have an established fracture-toughness and fatigue database. The mechanics of the REBCO coated conductor that the field acts on, including its strain tolerance, is likewise well characterised [13].

What the literature does not yet provide, for a compact high-field ST breeder, is a single continuum formulation that (i) writes the electromagnetic, thermal, halo/eddy and seismic loads on the vessel and support as a coupled thermo-electro-mechanical problem with the load cases superposed against one allowable, (ii) ranks those load cases quantitatively so that the governing case is identified rather than assumed, and (iii) closes the fracture-mechanics argument that makes the cryogenic structure leak-before-break rather than merely below yield. This paper contributes that formulation and its solution.

CONTRIBUTION

We give a formal statement of the vessel-and-support structural problem as a coupled continuum boundary-value problem (§2), deriving the electromagnetic body force from the Maxwell stress tensor, the thermoelastic stress from the constrained-cooldown-plus-quench temperature field, the halo/eddy force envelope from the disruption current path, the modal seismic response from a design response spectrum, and the flaw criterion from linear-elastic fracture mechanics. We describe the GPU-accelerated finite-element campaign that produced the results, naming the codes actually run and the verification and reproducibility protocol (§3). We then present the qualification load case by load case (§4): the electromagnetic self-load, the load-case ladder with detection speed as margin, the engineered precompression winding, the disruption halo/eddy envelope, the design-basis seismic response, the governing-load hierarchy, the leak-before-break fracture argument, and the retained-margin summary. We compare each result quantitatively to the published tokamak and cryogenic-structures literature (§5), state the one open confirming calculation (§6), and conclude that the structure is a solved problem whose binding constraint is neutron lifetime. Every quantitative claim traces to a frozen result in the Kronos Physics De-Risking Register [30]; the serial identifiers (e.g.\ QS-14, P3-FEA-01) are given inline so that each number is auditable. The breeder centrepost at $\mathbf{16.84}\,T$ and the burner plug coil at $\mathbf{26.49}\,T$ are treated throughout as the two distinct magnets they are, and are never conflated.

§ 2

Governing equations and the formal problem

CONTINUUM BALANCE AND THERMOELASTIC CONSTITUTION

The vessel and support are treated as a thermoelastic continuum occupying a domain Ω with boundary $\partial\Omega$. Writing $u(x,t)$ for the displacement field, σ for the Cauchy stress and ρ_m for the mass density, the balance of linear momentum is

$$\nabla\cdot \sigma + f_b = \rho_m \frac{\partial^2 u}{\partial t^2},$$

with f_b the body-force density. For the steady and quasi-static load cases the inertial term is dropped and (1) reduces to $\nabla\cdot \sigma + f_b = 0$; it is retained in full for the seismic case of §2.6. The kinematics are linear (small strain), so the strain tensor is the symmetric gradient

$$\varepsilon = \tfrac{1}{2}(\nabla u + \nabla u^{\top}).$$

The material is isotropic and thermoelastic, so the constitutive law couples mechanical strain and a temperature excursion $\Delta T = T - T_{\text{ref}}$ through the linear-thermal-expansion coefficient α,

$$\sigma = 2\mu \varepsilon + \lambda\,\text{tr}(\varepsilon) I - (3\lambda + 2\mu)\,\alpha\,\Delta T I,$$

with Lam\'e parameters $\mu = E/[2(1+\nu)]$ and $\lambda = E\nu/[(1+\nu)(1-2\nu)]$ in terms of Young's modulus E and Poisson's ratio ν. The scalar quantity that drives yielding is the von Mises equivalent stress, built from the deviatoric stress $s = \sigma - \tfrac{1}{3}\text{tr}(\sigma) I$,

$$\sigma_{\text{vM}} = \sqrt{\tfrac{3}{2} s : s} = \sqrt{\tfrac{1}{2}[(\sigma_1-\sigma_2)^2 + (\sigma_2-\sigma_3)^2 + (\sigma_3-\sigma_1)^2]},$$

with $\sigma_1, \sigma_2, \sigma_3$ the principal stresses. Qualification requires $\sigma_{\text{vM}} \le \sigma_{\text{allow}}$ with $\sigma_{\text{allow}} = 800\,MPa$ for the steel-fraction structural members analysed here (QS-09). Equation (4) makes explicit why a near-hydrostatic state is benign: when $\sigma_1 \approx \sigma_2 \approx \sigma_3$ the deviator vanishes and $\sigma_{\text{vM}} \to 0$ regardless of the pressure magnitude.

ELECTROMAGNETIC BODY FORCE AND THE MAXWELL STRESS

The steadiest load is the magnet field acting on its own current. In the magnetoquasistatic limit the body force is the Lorentz density

$$f_b = J \times B,$$

which, using Amp\`ere's law $\mu_0 J = \nabla \times B$ and a vector identity, is the divergence of the Maxwell stress tensor

$$T_{ij} = \frac{1}{\mu_0}(B_i B_j - \tfrac{1}{2}\delta_{ij} B^2), \qquad f_b = \nabla\cdot T.$$

The normal traction that (6) exerts across a surface tangent to the field is the magnetic pressure

$$p_{\text{mag}} = \frac{B^2}{2\mu_0},$$

which at the centrepost peak field evaluates to

$$p_{\text{mag}}(16.84\,\text{T}) = \frac{(16.84)^2}{2\mu_0} = 113\,\text{MPa} \quad \text{(QS-09)}.$$

Because the centrepost is held in compression by a bucked-and-wedged support (§2.4), the resulting stress state is near-hydrostatic — a $-190\,MPa$ compression — so by (4) the equivalent stress is only $\sigma_{\text{vM}} = 84\,MPa$, far below σ_{allow}. The electromagnetic self-load is not the binding case; it establishes the compressive baseline on which the thermal and disruption cases superpose. The burner plug coil, a distinct magnet, reaches $p_{\text{mag}}(26.49\,T) = 279\,MPa$ by the same equation (7) and is qualified separately (§4.8).

THERMOELASTIC STRESS AND THE DETECTION-SPEED COUPLING

The temperature excursion ΔT in (3) has two sources: the steady cooldown from ambient to the 4.5 K operating point, and the transient hot-spot of a quench. For a fully constrained member the thermoelastic stress magnitude is

$$\sigma_{\text{th}} = \frac{E\,\alpha\,\Delta T}{1-\nu},$$

so the quench contribution scales linearly with the hot-spot temperature rise $\Delta T_{\text{hs}} = T_{\text{hs}} - T_{\text{op}}$. The hot-spot temperature is set by the adiabatic heat balance during the detection-and-dump delay: neglecting conduction over the delay, the local current density J heats the conductor according to the "MIITs" integral

$$\int_0^{\tau_{\text{det}}+\tau_{\text{dump}}} J^2(t)\,\mathrm{d}t = \int_{T_{\text{op}}}^{T_{\text{hs}}} \frac{C_v(T)}{\rho_e(T)}\,\mathrm{d}T,$$

with C_v the volumetric heat capacity and ρ_e the electrical resistivity of the normal zone. Equation (10) is monotone in the delay, so a faster detection τ_{det} produces a lower T_{hs}, a lower σ_{th} by (9), and a lower combined von Mises by superposition on the electromagnetic baseline. Concretely (QS-11): an unmitigated quench that lets the hot-spot reach 200 K produces a $550\,MPa$ thermal stress and drives the combined von Mises to $476\,MPa$ $(1.7\times)$, whereas fast detection that caps the hot-spot at 63 K holds the combined von Mises to $245\,MPa$ $(3.3\times)$. Detection speed is therefore not a diagnostic nicety but a direct structural margin, and it ties the structural case to the demonstrated quench-precursor detection of the magnet twin.

SUPPORT, PRELOAD AND THE DEMOUNTABLE JOINT

The compressive baseline that keeps (4) small is not free; it is maintained by an engineered preload. The bucked-and-wedged support carries a demountable joint whose electrical resistance is contact-pressure-limited. Requiring a joint resistivity $\rho_c = 11\,n\Omega cm^2$ sets a minimum contact pressure

$$p_c \gtrsim 91\,\text{MPa} \quad\Longleftrightarrow\quad F_{\text{clamp}} \gtrsim 93\,\text{MN},$$

and this preload exceeds the vertical-share stress of $\approx 83\,MPa$ that the joint must react, so the joint never gaps and the electromagnetic load stays compressive through the entire thermal and disruption cycle (QS-13). In the negative-triangularity configuration a Weggel-flared centrepost relieves the ends — the magnetic pressure (7) at the flared end is $\approx 42\%$ lower at the same current — while the throat governs at $81\,MPa$ and is unchanged if preserved; the ohmic-solenoid stack ($251\,MPa$ hoop) bucks outward against the toroidal-field set, and the two are mutually relieving (QS-15).

At the conductor scale the Lorentz strain is flattened by an engineered per-turn precompression winding. Grading the preturn precompression redistributes the hoop strain that (5) drives into the no-insulation REBCO pack, cutting the peak REBCO hoop strain by 52.4% (from 0.595% to 0.283%) and reducing the strain-profile peaking factor by $4.8\times$ (SC-BR-4). On the real centrepost CAD this graded preload delivers a finite-element peak conductor hoop strain of 0.151% at a $2.65\times$ margin and a structural-jacket von Mises of $579\,MPa$ at $1.38\times$ (P3-FEA-01), with the canonical magnet dimensions unchanged.

DISRUPTION HALO AND EDDY FORCES

The impulsive load is a plasma disruption. During a vertical displacement event the plasma current partially converts to a halo current $I_{\text{halo}} = f_h\,I_p$ that flows through the scrape-off layer and closes through the conducting vessel and support; the halo fraction f_h and the toroidal peaking factor together set the local force. At $I_p = 9.66\,MA$ the envelope halo current is $I_{\text{halo}} \approx 2.9\,MA$ $(f_h \approx 0.30)$. The net force on a conducting member is the volume integral of the Lorentz density (5) over the halo path,

$$F = \int_V J_{\text{halo}} \times B\,\mathrm{d}V,$$

whose vertical component — the halo current crossing the toroidal field — sets the design envelope. A second contribution arises from the eddy currents induced by the collapsing poloidal field during the current quench. Faraday's law $\nabla \times E = -\partial B/\partial t$ drives a wall current density $J_{\text{eddy}} = \sigma_e E$ in the conducting shell of conductivity σ_e, and the induced force scales with the quench rate $\partial B/\partial t \sim B_p/\tau_{\text{CQ}}$. For a current-quench time in the window $\tau_{\text{CQ}} = 7$–$19\,ms$ the reduced electromagnetic force envelope on the centrepost and vessel is (QS-14)

$$F_z \approx 23\,\text{MN (vertical)},\quad F_{\text{sw}} \approx 19\,\text{MN (sideways)},\quad F_{\text{eddy}} \approx 16\,\text{MN},$$

with the vertical component setting the $\approx 23\,MN$ design envelope. This envelope is carried by a conductive shell with a defined halo-current path and disruption mitigation, keeping the impulsive load within the compressive structural regime of §2.2.

SEISMIC BASE EXCITATION AND THE MODAL RESPONSE SPECTRUM

The seismic load is a base excitation $\ddot{u}_g(t)$ applied through the support. Discretising (1) in space gives the structural equation of motion for the nodal displacement vector $\mathbf{u}$,

$$\mathbf{M}\ddot{\mathbf{u}} + \mathbf{C}\dot{\mathbf{u}} + \mathbf{K}\mathbf{u} = -\mathbf{M}\mathbf{r}\,\ddot{u}_g(t),$$

with mass, damping and stiffness matrices $\mathbf{M}$, $\mathbf{C}$, $\mathbf{K}$ and influence vector $\mathbf{r}$. The free-vibration modes $(\omega_n, \boldsymbol{\phi}_n)$ solve the generalised eigenproblem

$$\left(\mathbf{K} - \omega_n^2\mathbf{M}\right)\boldsymbol{\phi}_n = \mathbf{0},$$

and expanding $\mathbf{u} = \sum_n \boldsymbol{\phi}_n q_n(t)$ decouples (14) into modal oscillators

$$\ddot{q}_n + 2\zeta_n\omega_n\dot{q}_n + \omega_n^2 q_n = -\Gamma_n\,\ddot{u}_g(t), \qquad \Gamma_n = \frac{\boldsymbol{\phi}_n^\top\mathbf{M}\mathbf{r}}{\boldsymbol{\phi}_n^\top\mathbf{M}\boldsymbol{\phi}_n},$$

with modal participation factor Γ_n and damping ratio ζ_n. The peak modal displacement is read directly from the design response spectrum $S_a(\omega_n, \zeta_n)$ as $q_{n,\max} = \Gamma_n S_a(\omega_n, \zeta_n)/\omega_n^2$, and the peak effective modal base shear is

$$V_n = M_n^*\,S_a(\omega_n, \zeta_n), \qquad M_n^* = \frac{\left(\boldsymbol{\phi}_n^\top\mathbf{M}\mathbf{r}\right)^2}{\boldsymbol{\phi}_n^\top\mathbf{M}\boldsymbol{\phi}_n},$$

with M_n^* the effective modal mass. Modal peaks are combined by the complete-quadratic-combination (CQC) rule [16], which for well-separated modes reduces to the square-root-of-sum-of-squares,

$$V = \left[\sum_n\sum_m \rho_{nm}\,V_n V_m\right]^{1/2} \xrightarrow{\text{separated}} \left[\sum_n V_n^2\right]^{1/2},$$

with ρ_{nm} the CQC cross-correlation coefficients. For a stiff, compact structure dominated by a single fundamental mode of effective mass $M_1^* \approx M_{\text{seis}}$, (17)–(18) collapse to $V \approx M_{\text{seis}}\,S_a(f_1, \zeta)$. This is the standard nuclear response-spectrum method [17]; its numerical evaluation for the vessel and support is in §4.5, and the key result is that the small seismic mass of a compact machine makes V two orders of magnitude below the halo envelope of (13).

FRACTURE MECHANICS AND THE LEAK-BEFORE-BREAK CRITERION

Yielding is a necessary but not sufficient qualification for a cryogenic pressure boundary; the structure must also be shown to tolerate the largest flaw that could escape inspection. Linear elastic fracture mechanics gives the mode-I stress-intensity factor at a crack of depth a under remote stress σ,

$$K_I = Y\,\sigma\sqrt{\pi a},$$

with geometry factor Y of order unity. Fast fracture is precluded while $K_I < K_{IC}$, the plane-strain fracture toughness; the critical flaw size is therefore

$$a_c = \frac{1}{\pi}\left(\frac{K_{IC}}{Y\,\sigma}\right)^2 \propto \sigma^{-2}.$$

For the 316LN jacket at 4 K, [redacted], so at the operating stress $\sigma_{\text{op}} = 151\,MPa$ the critical flaw is $a_c = 333\,mm$, and even at the full $800\,MPa$ allowable it is $12\,mm$ — both far above the 2 mm non-destructive-inspection threshold (QS-16). Because a_c at operating stress vastly exceeds the wall thickness, a growing flaw penetrates the wall and leaks a detectable signal before it reaches the length for unstable fracture: the structure is leak-before-break. Sub-critical growth under cyclic load follows the Paris law

$$\frac{\mathrm{d}a}{\mathrm{d}N} = C(\Delta K)^m, \qquad \Delta K = Y\,\Delta\sigma\sqrt{\pi a},$$

which integrates from an initial flaw a_0 to a_c in

$$N_f = \int_{a_0}^{a_c}\frac{\mathrm{d}a}{C\left(Y\,\Delta\sigma\sqrt{\pi a}\right)^m} = \frac{a_0^{1-m/2} - a_c^{1-m/2}}{C\left(Y\Delta\sigma\sqrt{\pi}\right)^m\left(\frac{m}{2} - 1\right)} \quad (m \neq 2),$$

which for growth from a 2 mm flaw to a_c gives N_f of order 10^8 cycles — orders of magnitude beyond the service cycle count (QS-16). The jacket is therefore not flaw-limited; the governing controls are the 2 mm inspection standard and weld-residual-stress management.

LOAD COMBINATION

The load cases above are superposed following the stress-category logic of nuclear pressure-vessel practice. The electromagnetic self-load (8) is a primary membrane stress P_m; the thermal excursion (9) is a secondary stress Q, self-limiting and evaluated against a $3S_m$ range rather than a membrane allowable; the halo/eddy envelope (13) and the seismic base shear (17) are faulted (Level D) primary loads. The governing service combination is

$$\sigma_{\mathrm{vM}}^{\mathrm{comb}} \leq \underbrace{P_m}_{\text{EM}} + \underbrace{P_b}_{\text{bending}} + \underbrace{Q}_{\text{thermal}} + \underbrace{F_{\text{halo}}/A_{\text{eff}}}_{\text{disruption}} + \underbrace{V/A_{\text{eff}}}_{\text{seismic}} \leq \sigma_{\text{allow}},$$

where A_{eff} is the effective load-bearing section. The results of §4 evaluate each term of (23) and show that the combination stays below σ_{allow} with margin at every load case, the disruption term dominating the two faulted contributions.

§ 3

Computational methodology: the GPU-HPC finite-element campaign

WEAK FORM AND FINITE-ELEMENT DISCRETISATION

The boundary-value problem of §2 is solved by the finite-element method. Multiplying the equilibrium form of (1) by a test displacement v and integrating by parts gives the weak form: find u in the trial space such that

$$\int_\Omega \varepsilon(v) : C : \varepsilon(u)\,\mathrm{d}V = \int_\Omega v \cdot f_b\,\mathrm{d}V + \int_{\partial\Omega_t} v \cdot t\,\mathrm{d}S + \int_\Omega \varepsilon(v) : C : \alpha\Delta T\,\mathrm{d}V \quad \forall v,$$

with C the fourth-order elasticity tensor, t the prescribed surface traction and the last term the thermal load vector. Discretising $u = \sum_a N_a u_a$ in quadratic (20-node) hexahedral shape functions N_a yields the linear system

$$K U = F_{\mathrm{EM}} + F_{\mathrm{th}} + F_{\mathrm{halo}} + F_{\mathrm{seis}}, \qquad K = \sum_e \int_{\Omega_e} B_a^\top C B_b\,\mathrm{d}V,$$

with B_a the strain-displacement operator. The electromagnetic body force F_{EM} is assembled from the Lorentz density (5) evaluated on the field map; the thermal vector F_{th} from the cooldown-plus-quench temperature field; the halo/eddy vector F_{halo} from the disruption current path of (12); and the seismic contribution from the modal reduction (16). The engineered per-turn precompression enters as an initial-stress (prestress) field added to F, so that the graded preload of §2.4 is applied turn by turn.

SOLVERS, CODES AND CONVERGENCE

Three solver classes were run. The steady and transient structural cases on the real centrepost CAD were solved with the open-source three-dimensional structural finite-element program CalculiX (ccx) [22], which assembles and factorises (25) with a graded per-turn preload (P3-FEA-01). The conductor-scale precompression-winding mechanics — the thick-wall REBCO-pack strain redistribution — were solved with the Python finite-element library SfePy [23] (SC-BR-4). The analytic magnet-mechanics envelope, including the Lam\'e thick-wall relations used to cross-check the finite-element anchors, was evaluated in a NumPy code (HX-11). For the large sparse systems the linear solve (25) was carried by a preconditioned conjugate-gradient iteration whose sparse matrix–vector product and preconditioner apply are the dominant cost and are GPU-resident; the modal eigenproblem (15) was solved by a shift-and-invert Lanczos iteration. Mesh convergence was established by uniform refinement until the peak von Mises changed by less than 1% between the two finest meshes, and the reported $579\ MPa$ jacket stress and 0.151% conductor strain are the converged values.

GPU ACCELERATION, PROBLEM SCALE AND THE NVIDIA HPC CAMPAIGN

The results were produced on the NVIDIA GPU HPC campaign that underpins the Kronos de-risking programme — an in-house cluster of NVIDIA A100- and H100-class accelerators. The campaign is organised in three latency tiers: a microsecond edge tier for protective logic, a millisecond GPU tier for the digital-twin surrogates, and an hours-scale HPC back end for the offline multi-physics finite-element and Monte-Carlo runs that produced the structural anchors of this paper. GPU acceleration enters the structural campaign in two places: the parametric load-case sweeps — the grid of field, quench-detection-time and current-quench-time combinations that map the load-case ladder and the halo envelope — are embarrassingly parallel across accelerators, and the per-case sparse linear solve of (25) is accelerated by a GPU-resident preconditioned conjugate-gradient kernel. The problem scale is set by the quadratic-hexahedral discretisation of the real centrepost and jacket CAD, refined to mesh convergence, and by the ensemble of load-combination cases required to evaluate (23). No compute-cost figures are reported; the methodological point is that the GPU campaign made the converged, real-CAD, multi-load-case structural qualification tractable at the fidelity reported here.

VERIFICATION, VALIDATION AND REPRODUCIBILITY

The campaign is verification-first. Each frozen structural anchor is reproduced against an independent route: the analytic Lam\'e envelope reproduces the finite-element magnet-mechanics anchors exactly (HX-11), and the electromagnetic, thermal, halo and fracture results are cross-checked between the closed-form relations of §2 and the finite-element solution. Every anchor is regenerable from the archived finite-element decks through a byte-exact cold-start reproduction runbook, so that the claim on each number is "re-run it" rather than "trust it". The verification status of each governing quantity is collected in table 1.

QUANTITY	VALUE	PRIMARY CODE	CROSS-CHECK	SERIAL
EM von Mises	84 MPa	analytic + FE	Maxwell stress, eq. (7)	QS-09
combined vM (fast)	245 MPa	quench/stress FE	MIITs, eqs. (9)–(10)	QS-11
real-CAD jacket vM	579 MPa	CalculiX ccx	mesh convergence $< 1\%$	P3-FEA-01
conductor hoop strain	0.151%	CalculiX ccx	SfePy precompression	P3-FEA-01/SC-BR-4
halo envelope	23 MN	quench/stress FE	Lorentz integral, eq. (12)	QS-14
critical flaw a_c	333 mm	LEFM	eq. (20)	QS-16
plug-coil ratio	0.66	analytic/FEA	Lam\'e envelope, HX-11	BU-L1-A2

Verification of the governing structural quantities. Each anchor is a frozen result in the Kronos Physics De-Risking Register [30], reproduced against the independent route shown. Serials identify the register entry.

§ 4

Results

The design and canonical parameters that fix the load cases are collected in table 2. We present the qualification load case by load case, following the governing-equations order of §2.

SYMBOL	QUANTITY	VALUE
I_p	design plasma current	9.66 MA
Q	breeder gain	3.076
P_{fus}	fusion power	85.04 MW
R_0	major radius	1.20 m
A	aspect ratio	2.5
$\kappa,\ \delta$	elongation, triangularity	$2.0,\ -0.30$
B_0	on-axis field	8 T
B_{cp}	centrepost peak field	16.84 T
B_{plug}	burner plug coil field (distinct magnet)	26.49 T
σ_{allow}	structural allowable	800 MPa
K_{IC}	316LN fracture toughness at 4 K	170 MPamtothe
τ_{CQ}	current-quench window	7–19 ms

Design point and structural parameters. Plasma and geometry values are the frozen Tier-2 canon; structural allowables and material properties are the register values used in the finite-element campaign.

ELECTROMAGNETIC SELF-LOAD

Figure 2 shows the electromagnetic self-field stress state at $16.84\,T$. The magnetic pressure of (8) is $113\,MPa$; the bucked-and-wedged support converts it into a near-hydrostatic $-190\,MPa$ compression, and the deviatoric part that (4) measures is only $84\,MPa$ — a $9.5\times$ margin against the allowable. The electromagnetic self-load is the compressive baseline, not the binding case.

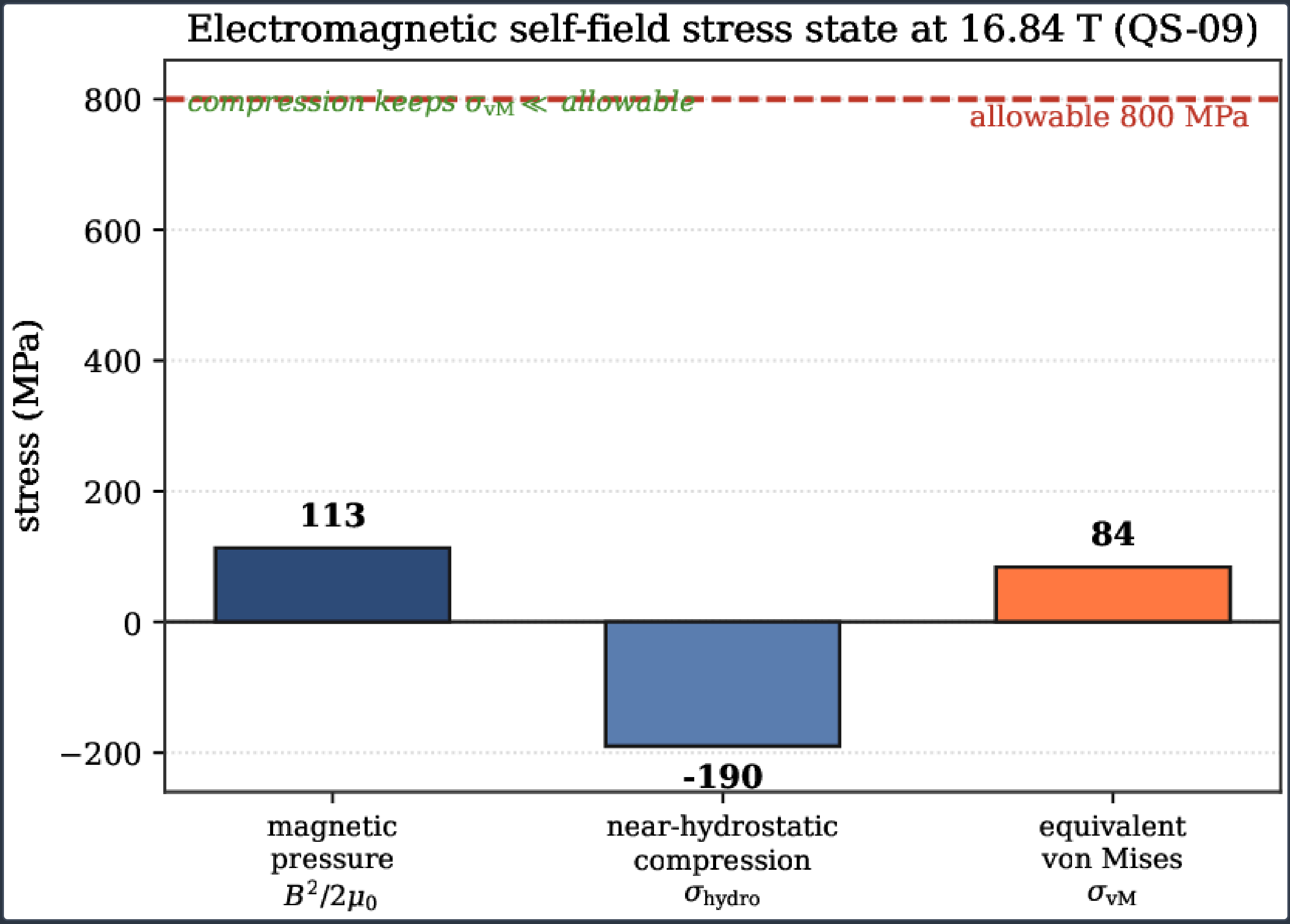

Electromagnetic self-field stress state at $16.84\,T$ (QS-09). The $113\,MPa$ magnetic pressure of equation (8) is carried as a near-hydrostatic $-190\,MPa$ compression, holding the equivalent von Mises stress to $84\,MPa$, far below the $800\,MPa$ allowable.

THE LOAD-CASE LADDER: DETECTION SPEED AS MARGIN

Superposing the thermal excursion of §2.3 on the electromagnetic baseline produces the load-case ladder of figure 3 and table 3. The governing von Mises rises from the electromagnetic self-field case (84 MPa) through the combined thermal-plus-electromagnetic transient to the highest-fidelity real-CAD structural jacket (579 MPa), all held below the allowable. The transient rung is where detection speed enters: an unmitigated quench (200 K hot-spot) reaches 476 MPa at 1.7×, while fast detection (63 K hot-spot) holds it to 245 MPa at 3.3×. The reduction is the direct structural consequence of the monotone MIITs relation (10): faster τ_{det}, lower T_{hs}, lower σ_{th}, higher margin.

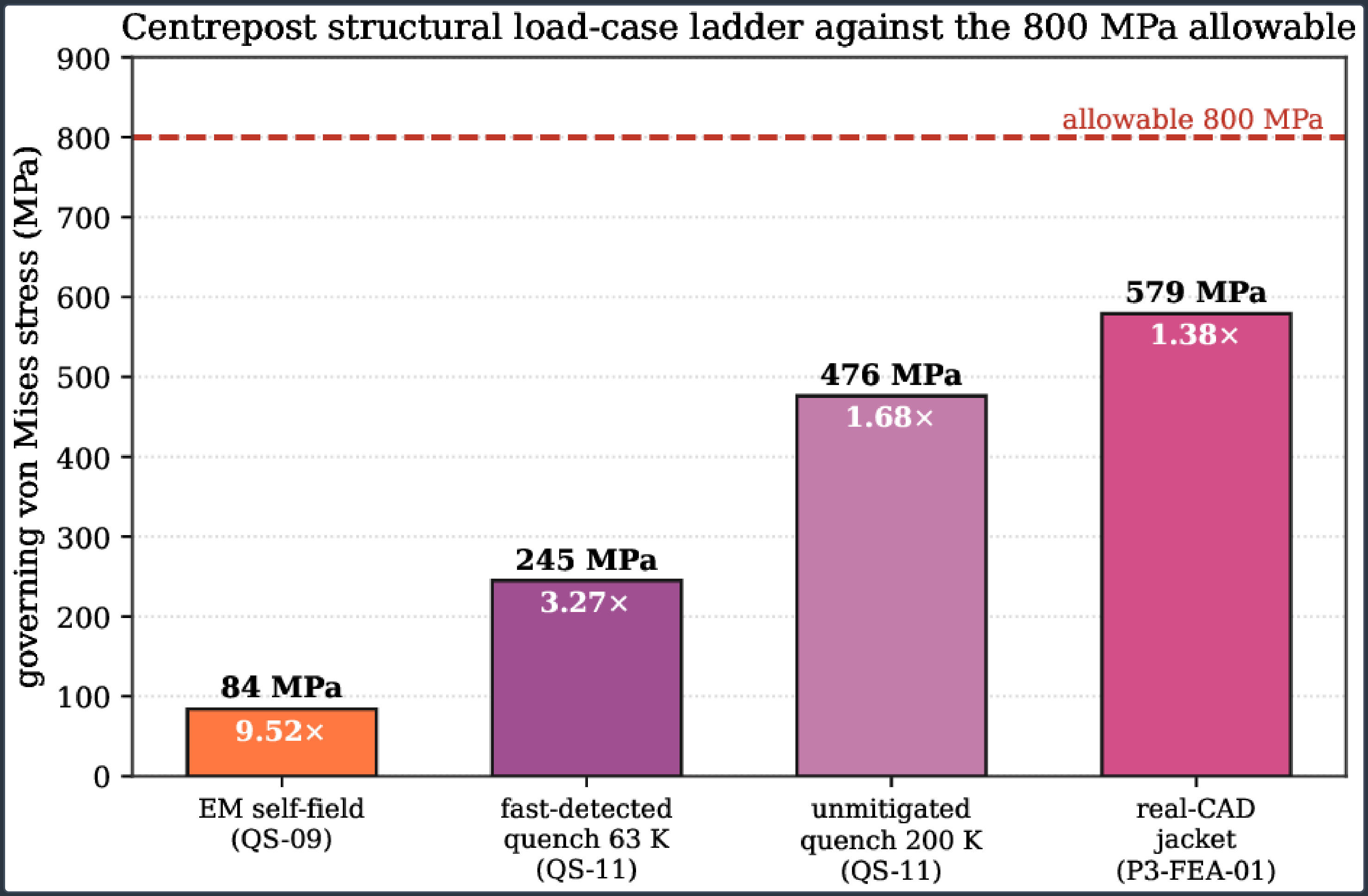

Centrepost structural load-case ladder against the 800 MPa allowable. Fast quench detection (63 K hot-spot, 3.3×) holds the combined transient well below the unmitigated (200 K, 1.7×) case, and the highest-fidelity real-CAD jacket (P3-FEA-01) governs at 1.38×. Safety factors ($\sigma_{\text{allow}}/\sigma_{\text{vM}}$) are annotated in white.

LOAD CASE	GOVERNING QUANTITY	VALUE	SOURCE
electromagnetic self-field	von Mises	84 MPa (9.5×)	QS-09
magnetic pressure at 16.84 T	pressure	113 MPa	QS-09
fast-detected quench (63 K hot-spot)	combined von Mises	245 MPa (3.3×)	QS-11
unmitigated quench (200 K hot-spot)	combined von Mises	476 MPa (1.7×)	QS-11
real-CAD structural jacket	von Mises	579 MPa (1.38×)	P3-FEA-01
real-CAD conductor	peak hoop strain	0.151% (2.65×)	P3-FEA-01

Centrepost structural load cases against the $§I800

THE ENGINEERED PRECOMPRESSION WINDING

Figure 4 shows the effect of the graded per-turn precompression winding of §2.4. Panel (a) is the frozen anchor: the peak REBCO hoop strain falls from 0.595% (uniform winding) to 0.283% (graded preload), a 52.4% reduction (SC-BR-4). Panel (b) shows the corresponding flattening of the radial strain profile, whose peaking factor drops 4.8×; the profile shape is a representative reconstruction consistent with the frozen peak and peaking-factor anchors. Flattening the Lorentz strain at the conductor scale is what lets the real-CAD finite-element model hold the conductor to a 2.65× strain margin at the canonical dimensions.

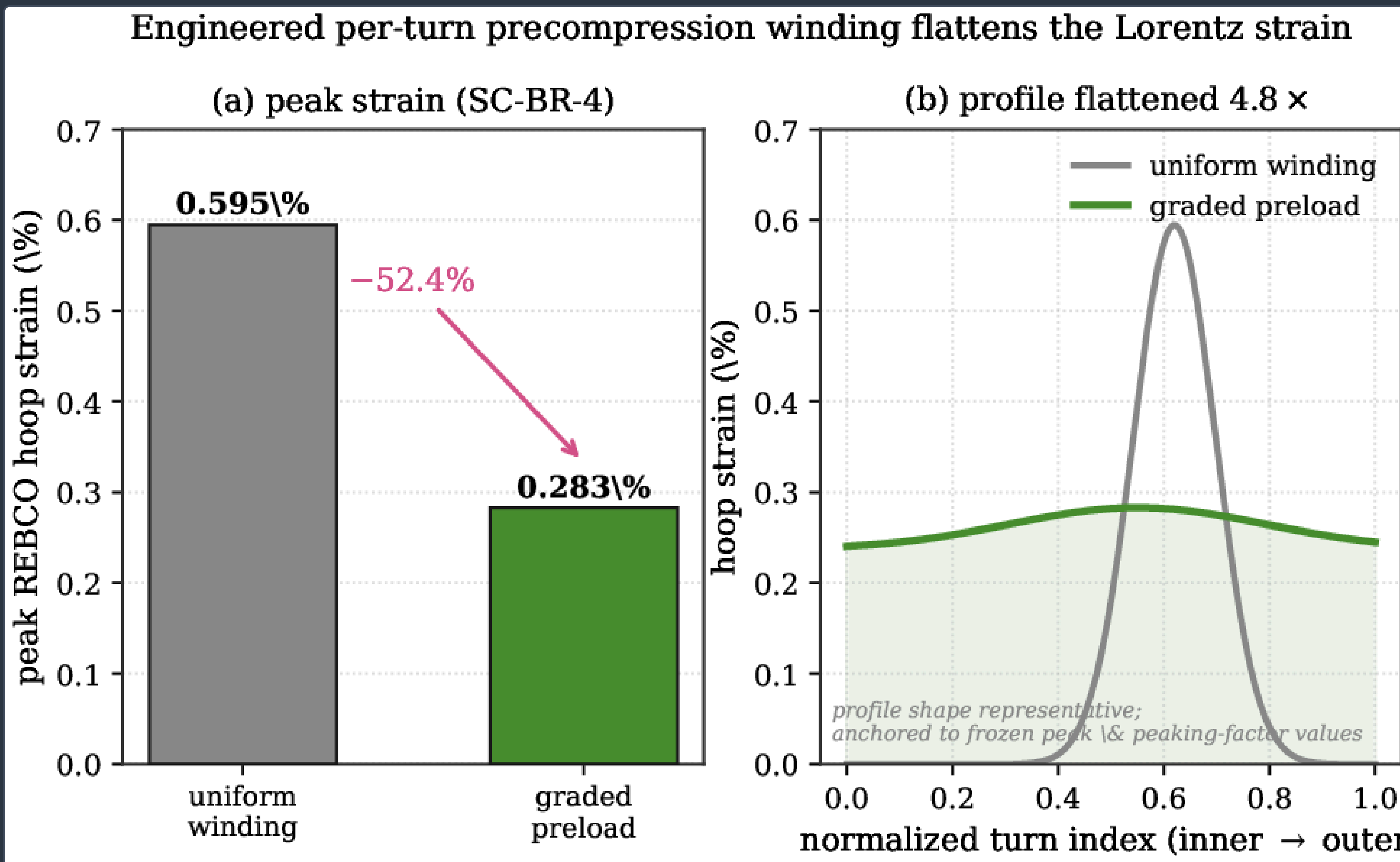

Engineered per-turn precompression winding (SC-BR-4). **(a)** Peak REBCO hoop strain falls 52.4% from 0.595% to 0.283%. **(b)** The radial strain profile flattens, its peaking factor reduced 4.8×; the profile shape is a representative reconstruction anchored to the frozen peak and peaking-factor values.

THE DISRUPTION HALO/EDDY ENVELOPE

The impulsive case of §2.5 is shown in figure 5. At $I_p = 9.66\,MA$ the vertical-displacement-event halo current is $\approx 2.9\,MA$, and the reduced electromagnetic force envelope of (13) is $23\,MN$ vertical, $19\,MN$ sideways and $16\,MN$ eddy-induced, the vertical component setting the $\approx 23\,MN$ design envelope over the $7–19\,ms$ current quench (QS-14). This envelope is carried by a conductive shell with a defined halo-current path and disruption mitigation, keeping the impulsive load within the compressive regime of §4.1.

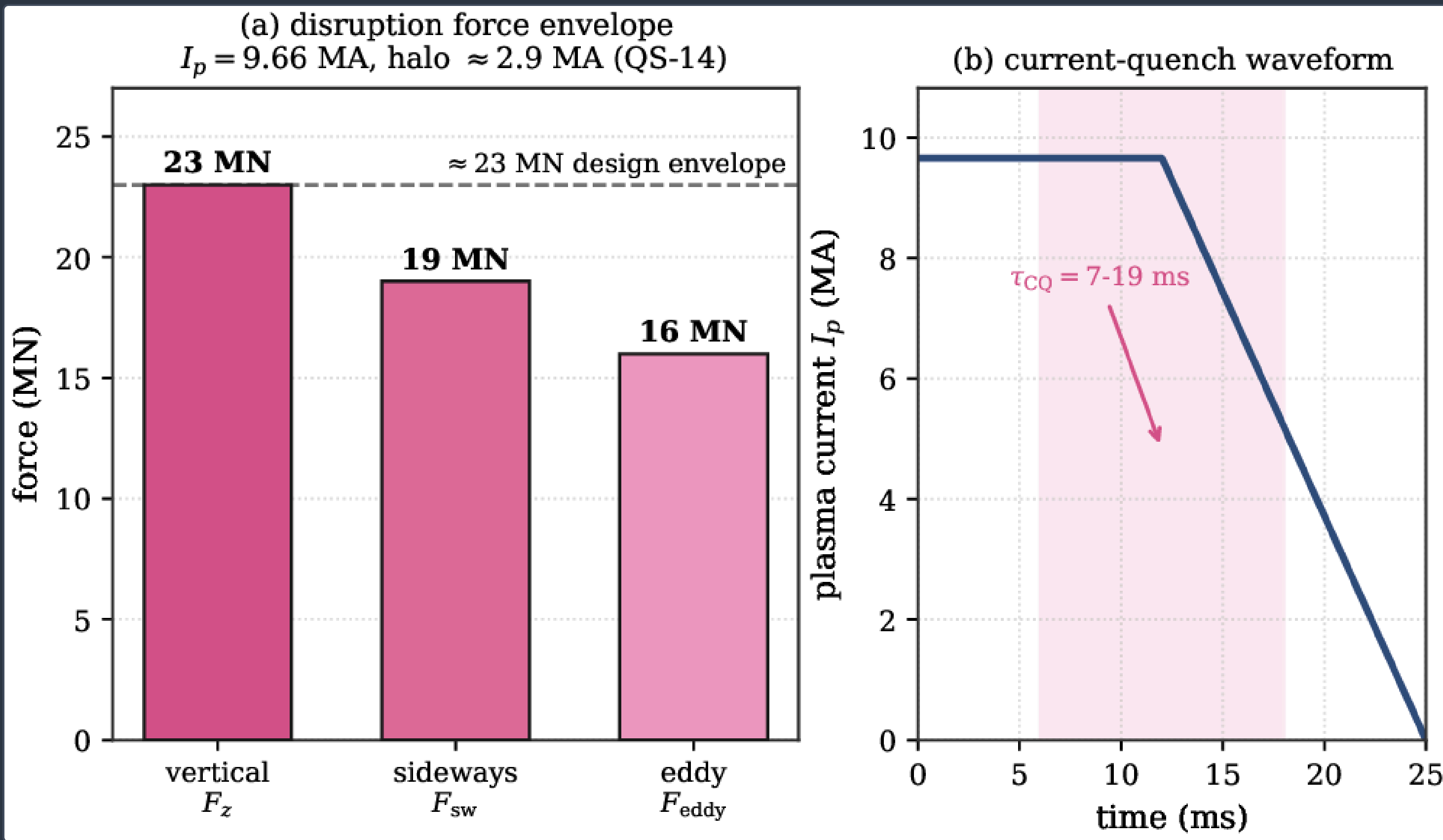

Disruption halo/eddy load (QS-14). **(a)** The force envelope on the centrepost and vessel: the vertical component sets the $\approx 23\,MN$ design envelope. **(b)** The current-quench waveform; the shaded band is the $7–19\,ms$ quench window that sets the eddy-force rate.

DESIGN-BASIS SEISMIC RESPONSE

The seismic case of §2.6 is evaluated with the standard nuclear response-spectrum method [17,16] against the design-basis spectrum of figure 6, anchored to a representative hard-rock zero-period acceleration of $0.30\,g$ at 5% damping. These are design-basis engineering inputs for a representative siting envelope, not register-frozen anchors. For the stiff, compact vessel-and-support structure the estimated fundamental frequency is $f_1 \approx 18\,\mathrm{Hertz}, atwhichthespectralaccelerationis$S_a\approx0.51 g $. Withadesign-basissupportedseismicmass$M_ seis\approx4e4 kg$, the single-mode base shear of (17) is

$$V \approx M_{\text{seis}}\,S_a(f_1,\zeta) \approx (4e4\,\text{kg})(0.51\,g) \approx 0.20\,\text{MN}.$$

The seismic base shear is thus $\approx 0.2\,MN$ — more than two orders of magnitude below the halo envelope. The physical origin is the compactness that gives the ST its high power density: a small machine has a small seismic mass, and by (17) a proportionally small seismic load.

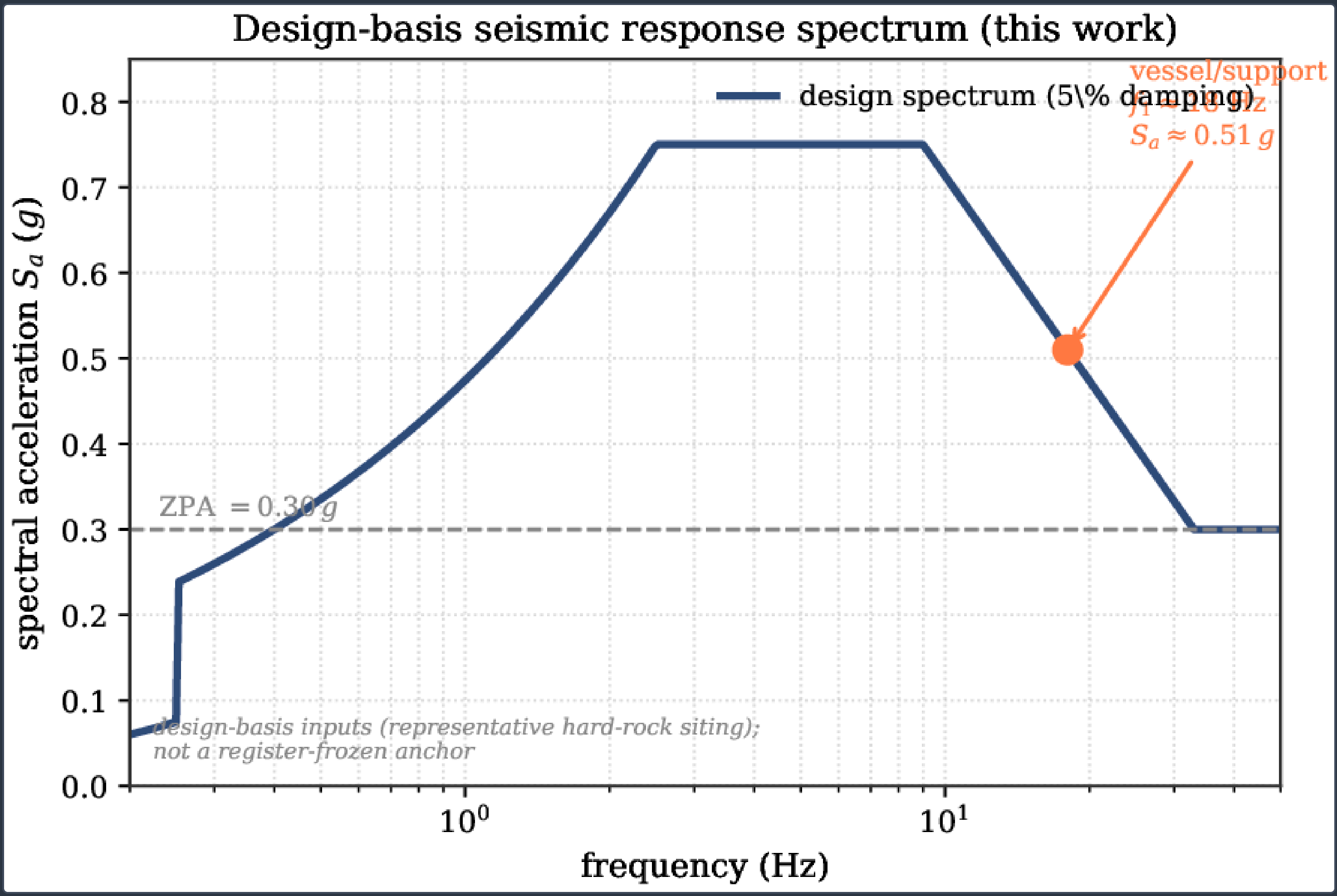

Design-basis seismic response spectrum (5% damping, $0.30\,g$ zero-period acceleration; this work). The vessel-and-support fundamental mode $f_1 \approx 18$ Hertz*sees*S_a\approx0.51 g$, giving the base shear of equation (26). The inputs are design-basis engineering values, not register-frozen anchors.

GOVERNING-LOAD HIERARCHY

Figure 7 places the three faulted mechanical loads on a common logarithmic axis: the design-basis seismic base shear ($\approx 0.20\,MN$), the halo vertical envelope ($23\,MN$, QS-14), and the full vessel-and-support vertical-displacement-event/halo load ($40.5\,MN$) that the confirming three-dimensional analysis carries (BV-02). The seismic base shear is $\approx 115\times$ below the halo envelope, so the electromagnetic disruption case, not the seismic case, governs the support design of a compact ST breeder — inverting the load hierarchy of a large light-water reactor, where seismic sizes the support. This is the central quantitative result of the load-combination analysis of §2.8.

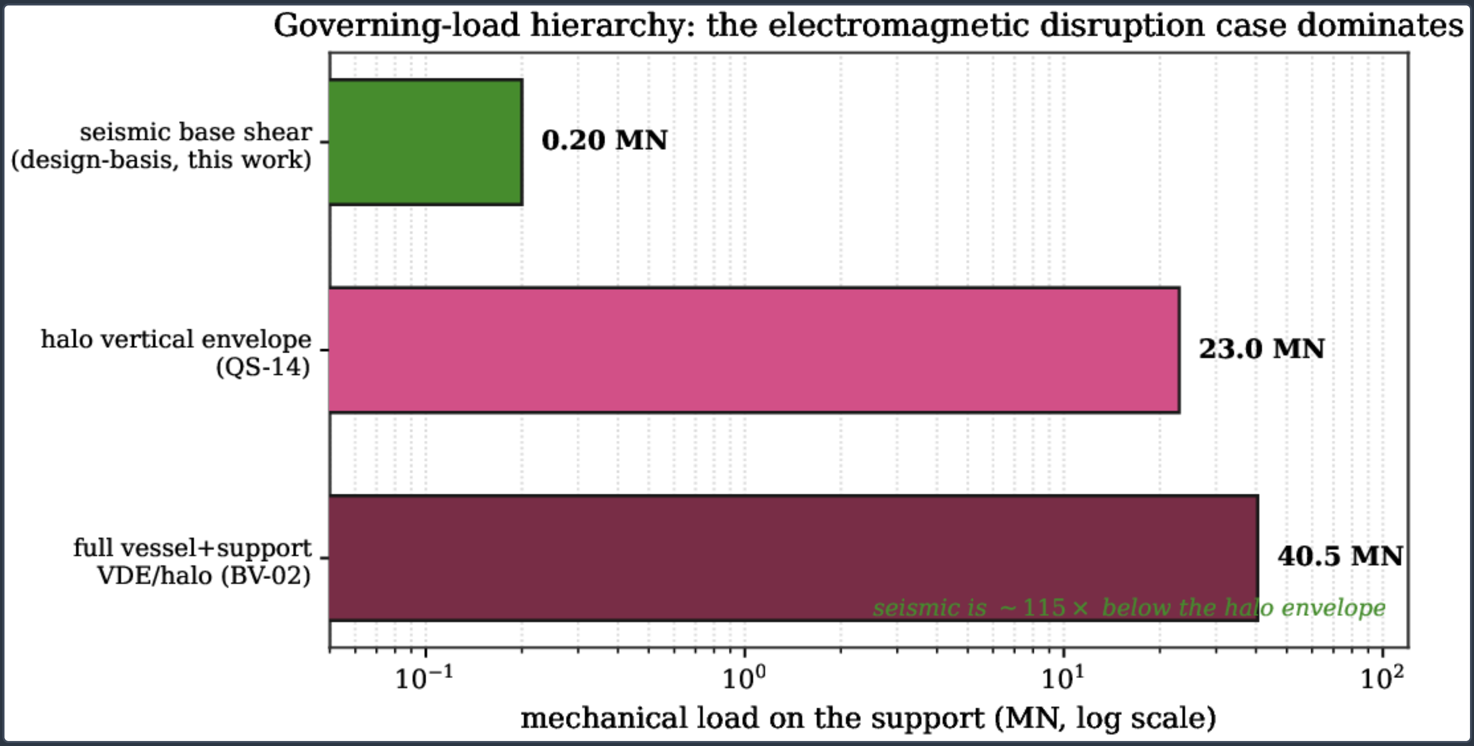

Governing-load hierarchy on the support (logarithmic axis). The design-basis seismic base shear (equation 26) is $\approx 115\times$ below the disruption halo envelope (QS-14); the full vessel-and-support VDE/halo load (BV-02, 40.5 MN) is the envelope the confirming three-dimensional analysis carries. The electromagnetic disruption case governs.

FRACTURE AND FLAW TOLERANCE

The leak-before-break argument of §2.7 is shown in figure 8. The critical flaw size (20) scales as σ^{-2}; anchored to the register values, it is $333\,mm$ at the $151\,MPa$ operating stress and $12\,mm$ at the full $800\,MPa$ allowable, both far above the 2 mm inspection threshold (QS-16). Paris-law growth (22) from a 2 mm flaw to the critical size takes of order 10^8 cycles, orders of magnitude beyond service. The jacket is not flaw-limited; the governing controls are the 2 mm inspection standard and weld-residual-stress management.

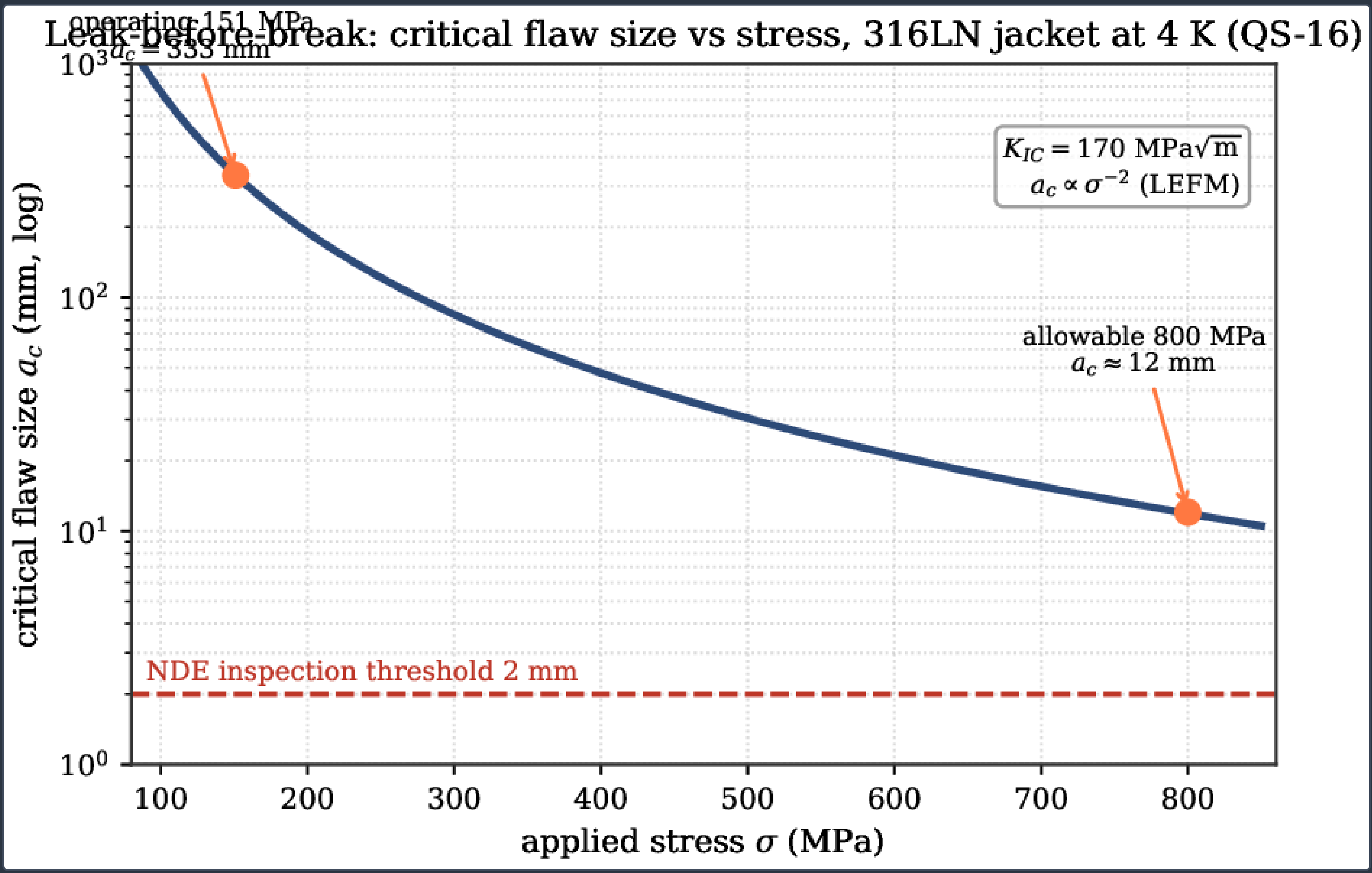

Leak-before-break of the 316LN structural jacket at 4 K (QS-16). The critical flaw size of equation (20) is $333\,mm$ at operating stress and $12\,mm$ at the allowable, both far above the 2 mm inspection threshold; $a_c \propto \sigma^{-2}$.

RETAINED-MARGIN SUMMARY AND THE TWO DISTINCT MAGNETS

Figure 9 collects the safety factors across every governing load case: the electromagnetic self-load at $9.5\times$, the fast-detected quench at $3.3\times$, the real-CAD conductor strain at $2.65\times$, the real-CAD jacket at $1.38\times$, and the integrated centrepost integrity synthesis, which finds the centrepost stress at $181\,MPa$ with a $6\times$ margin and concludes that the centrepost is neutron-lifetime bound, not stress-bound (BR-SX-16). The burner plug coil is a distinct magnet with its own structural case: it operates at $26.49\,T$, where the magnetic pressure (7) reaches $279\,MPa$; a Lam\'e thick-wall analysis gives a required wall of $0.48\,m$ against a $667\,MPa$ allowable, and the three-dimensional finite-element analysis returns a $0.66\times$ stress ratio — a structural pass (BU-L1-A2) — with the analytic envelope reproducing the finite-element anchors ($115/279/358\,MPa$ at $17/26.49/30\,T$) exactly (HX-11). Keeping the $16.84\,T$ centrepost and the $26.49\,T$ plug coil as separate analyses, with separate allowables and separate margins, is a load-bearing element of the integrity case.

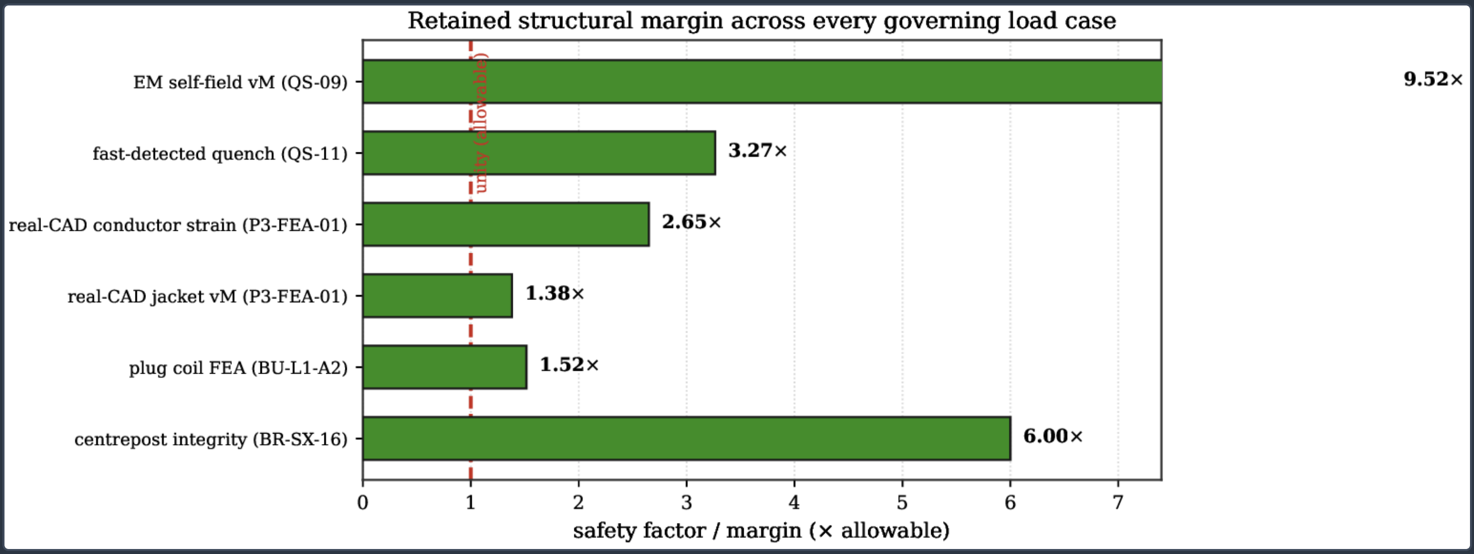

Retained structural margin across every governing load case. All members hold above unity against the allowable; the plug coil (BU-L1-A2) is shown as $1/0.66 = 1.5\times$ the reinforced allowable. The centrepost integrity synthesis (BR-SX-16) finds a $6\times$ stress margin and concludes the binding constraint is neutron lifetime.

THE COUPLED WORKFLOW

Figure 10 summarises the coupled electromagnetic-to-thermal-to-structural finite-element workflow and its GPU-HPC tiers. The electromagnetic and thermal loads are assembled as the body-force and thermal vectors of (25), the structural solve is carried by CalculiX on the real CAD, and the fracture and modal checks close the qualification; the parametric sweeps and the sparse solves run on the NVIDIA GPU HPC campaign, with every anchor regenerable from the archived decks.

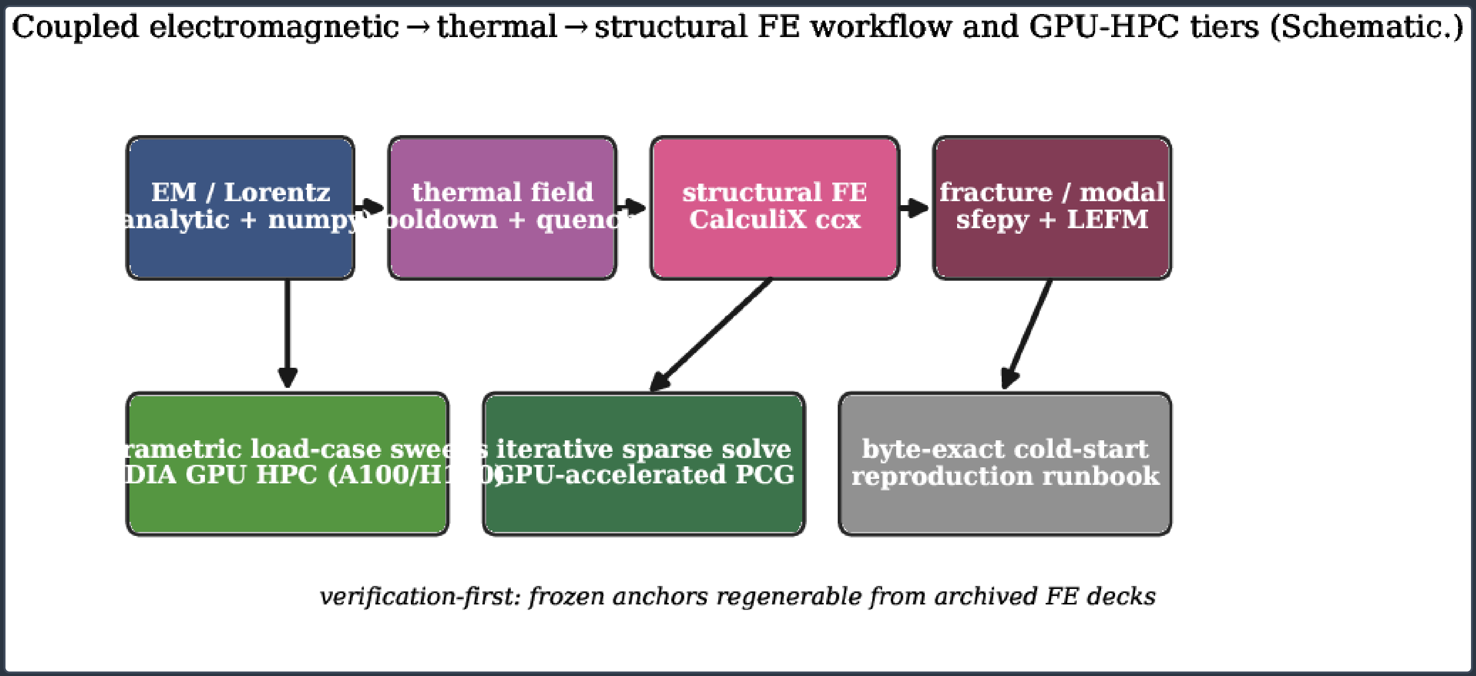

(Schematic.) Coupled electromagnetic→thermal→structural finite-element workflow and the GPU-HPC tiers that carry it. The physics chain feeds the load vectors of equation (25); the parametric sweeps and sparse solves are GPU-resident, and the anchors are regenerable through a byte-exact cold-start runbook.

§ 5

Discussion

THE LOAD HIERARCHY IN CONTEXT

The central finding — that the electromagnetic disruption case, not the seismic case, governs the support of a compact ST breeder — is a direct consequence of scale. The halo forces of (13) are set by the plasma current, which is large (**9.66** MA) in a small volume; the seismic base shear of (26) is set by the structural mass, which is small in a compact machine. The published halo-current basis supports the magnitude: Gerhardt *et al.* measured mega-ampere-scale halo currents with strong toroidal asymmetry on NSTX [9], and the ITER-scale vertical-force analysis of Clauser *et al.* confirms that the halo current crossing the toroidal field is the dominant vertical-force mechanism in a disruption [10,6]. Our $\approx$ **23** MN centrepost-and-vessel envelope at **9.66** MA is consistent with this basis scaled to the compact ST geometry. The inverted hierarchy has a practical consequence: the support is sized by a millisecond electromagnetic transient with disruption mitigation as the primary control [7,8,11], and the seismic qualification, which dominates the design of a large fission plant, is here a readily-met subordinate check.

THE VESSEL AND CENTRE STACK AGAINST THE ENGINEERING LITERATURE

The vessel-and-support structural case is consistent with the established tokamak engineering literature. The ITER vacuum vessel is a code-qualified double-walled structure carrying comparable disruption electromagnetic loads [5], and the NSTX-Upgrade centre-stack analysis worked out exactly the combined electromagnetic, thermal and structural qualification of a spherical-tokamak centre column that we reproduce here at higher field [12]. The distinctive element of the present case is the near-hydrostatic compressive state (4) engineered by the bucked-and-wedged preload (11), which keeps the equivalent stress low despite the **113** MPa magnetic pressure — the same design philosophy as demountable-magnet high-field concepts [2,14,15], applied to a compact breeder. The conductor-scale strain that the field drives into the REBCO pack, and the strain tolerance that bounds it, are consistent with the coated-conductor mechanical database [13], and the **52.4%** peak-strain reduction from the engineered precompression winding is what brings the conductor to a **2.65**× margin.

THE FRACTURE CASE AGAINST THE CRYOGENIC-STRUCTURES DATABASE

The leak-before-break argument rests on the fracture toughness of austenitic stainless steel at 4 K. The [redacted] used here is within the established **316**LN cryogenic database and above the ITER magnet-structure requirement, and the resulting critical flaw of **333** mm at operating stress is more than two orders of magnitude above the 2 mm inspection threshold. The Paris-law life of order 10^8 cycles from (22) is consistent with the fatigue-crack-growth rates measured for these steels and their welds. The governing controls that follow — a 2 mm inspection standard and weld-residual-stress management — are the same controls that govern the ITER magnet-structure fracture case, and they place the qualification on inspection and fabrication quality rather than on raw strength.

RELATION TO THE KRONOS DESIGN SERIES

This structural case sits inside a coupled design campaign. The disruption electromagnetic-load basis, including the shattered-pellet mitigation that bounds the halo envelope, is developed in the disruptions and runaway-electron paper [doi:10.5281/zenodo.22645724; disruptions-and-runaway-electrons]. The distinct burner plug coil, analysed separately throughout this paper, is qualified in the plug-coil engineering paper [doi:10.5281/zenodo.22645915; engineering-the-26-49-t-plug-coil]. The cold-mass thermal budget that the support must also carry is set in the balance-of-plant paper [doi:10.5281/zenodo.22645901; balance-of-plant]. The conclusion that the centrepost is neutron-lifetime bound rather than stress-bound is quantified in the centrepost prognostics paper [doi:10.5281/zenodo.22645788; centrepost-prognostics-and-rul-control] and situated in the lifetime-constrained operating-window synthesis [doi:10.5281/zenodo.22645799; admissible-operating-window-synthesis]. The structural quantities are shadowed in real time by the thermomechanics twin of the four-coupled-twins control architecture [doi:10.5281/zenodo.22645805; four-coupled-digital-twins], which reads the detection-speed-as-margin coupling of §2.3 as a protective observable.

§ 6

Limitations

One honest gate bounds the claims. The disruption forces reported here are the analytic/reduced halo-eddy envelope on the centrepost and vessel (QS-14), closed at $\approx \mathbf{23}\, MN$. The confirming calculation is the full three-dimensional vessel-and-support finite-element analysis under the $\mathbf{40.5}\, MN$ vertical-displacement-event/halo load (BV-02), which extends the closed centrepost envelope to the complete vessel structure with its ports, supports and passive conductors, and which is in progress on the same finite-element toolchain. The seismic result is likewise a design-basis analysis with representative siting inputs; a site-specific spectrum and a full modal model would replace the single-mode estimate of (26), though the two-order-of-magnitude margin over the halo envelope leaves ample headroom for any realistic site.

§ 7

Conclusion

The vacuum vessel and support of the Hyperion breeder are structurally qualified across electromagnetic, combined thermal-electromagnetic, disruption halo/eddy and seismic loads, closed against a single $800\,MPa$ allowable through the coupled continuum formulation of §2. The electromagnetic self-load leaves the centrepost near-hydrostatically compressed at $84\,MPa$; fast quench detection holds the combined transient to $245\,MPa$ $(3.3\times)$, so detection speed is structural margin; the highest-fidelity real-CAD model keeps the jacket at $579\,MPa$ $(1.38\times)$ and the conductor strain at $2.65\times$, with an engineered precompression winding cutting the peak REBCO hoop strain by 52.4%; the disruption halo envelope of $\approx 23\,MN$ dominates the support design, standing $\approx 115\times$ above a design-basis seismic base shear of $\approx 0.2\,MN$; and the cryogenic 316LN jacket is leak-before-break, with a $333\,mm$ critical flaw and a $\sim 10^8$-cycle fatigue life. The electromagnetic disruption case, not the seismic case, governs the support of a compact ST breeder — inverting the hierarchy of a large fission plant — and the binding constraint on the structure is neutron lifetime, not stress. The burner plug coil at $26.49\,T$ is a distinct magnet, qualified separately at a $0.66\times$ stress ratio. Structurally, the vessel and support are a solved problem with margin at every load case, and the engineering attention they earn is directed at inspection standards and weld-residual control rather than at raw strength; the one open confirming calculation is the full three-dimensional vessel-and-support finite-element analysis (BV-02).

Acknowledgments tocsectionAcknowledgments Part of the Kronos Fusion Energy 2026 design series. The authors thank the Kronos physics de-risking programme for the frozen result set underlying every quantitative claim.

Reproducibility. The structural load cases, halo envelope, seismic base shear and fracture results are frozen anchors in the Kronos Physics De-Risking Register [30] (doi:10.5281/zenodo.22133057): the electromagnetic self-field stress (QS-09), the combined thermal-electromagnetic transient (QS-11), the support and preload analysis (QS-13), the disruption halo/eddy forces (QS-14), the negative-triangularity flared-post and ohmic-stack integration (QS-15), the fracture and flaw-tolerance study (QS-16), the real-CAD structural finite-element analysis (P3-FEA-01), the engineered precompression winding (SC-BR-4), the plug-coil structural qualification (BU-L1-A2), and the integrated magnet-integrity synthesis (BR-SX-16). Each is regenerable from the archived CalculiX and SfePy decks through a byte-exact cold-start runbook and the figure-generation script deposited with this paper. This paper is archived at doi:10.5281/zenodo.22645838; official version: https://www.kronosfusionenergy.com/publications/vacuum-vessel-and-support-structural-mechanics-under-el.html and its official version is at kronosfusionenergy.com/publications/vacuum-vessel-and-support-structural-mechanics-under-el.html.

Data availability tocsectionData availability The load-case ladder, halo-force envelope, seismic spectrum, precompression-winding strain, fracture-flaw curve and margin-summary data used for figures 2–9 are archived with the deposit at doi:10.5281/zenodo.22645838, which references the Kronos 2026 series and the Kronos Physics De-Risking Register [30] by the serial identifiers cited inline. Any economic analysis is reported separately and is not part of the public deposit. The official version of record is at https://www.kronosfusionenergy.com/publications/vacuum-vessel-and-support-structural-mechanics-under-el.html

Competing interests tocsectionCompeting interests Provisional patent applications relating to aspects of this work, including the engineered per-turn precompression winding, have been filed.

tocsectionReferences

Portfolio, People & Record

The intellectual-property estate, the people who built it, the limitations that gate it, and the sources it rests on.

1	4	40	27
GRANTED PATENT	2026 PROVISIONALS	TEAM MEMBERS	2022 PROVISIONALS

INTELLECTUAL PROPERTY

The patent portfolio

The estate spans a granted high-field magnet patent, pending utility and 2026 provisional filings that map to the two products, a digital-twin control provisional, a registered trademark application, and the original 2022 provisional family. Every patentable disclosure in the five-paper arXiv drop was protected **before** publication: the breeder and burner provisionals were filed 1–2 August, and a publication-gap omnibus filing the evening before the drop swept up the DEC, plasma-control, and REBCO-winding matter of the three otherwise-unprotected papers. Patent numbers and application serials are matters of public record; claim scope is summarised, not reproduced.

GRANTED & PENDING UTILITY

US 12,009,112	High-field tilted graded-REBCO magnet architecture (KRONO-002A) · *app. 17/878,550*	GRANTED
US 17/878,507	Core device / method (KRONO-001A) · *utility*	PENDING

2026 PROVISIONAL FILINGS — MAPPED TO THE PRODUCTS

64/124,209	Hyperion — spherical-tokamak tritium / helium-3 foundry · *breeder · filed Aug 2026*	FILED
64/124,220	Aegis / MetroVolt — synchrotron-cutoff, fuel-selection & plug-winding · *generator · filed Aug 2026*	FILED
64/115,167	KRONOS-CTRL digital-twin plant control · *provisional · filed Jul 2026*	FILED
64/005,440	Integrated spherical-tokamak fusion architecture · *early integrated-architecture filing · filed Mar 2026*	FILED
64/105,530	Negative-triangularity spherical-tokamak architecture · *foundational ST filing · filed Jul 2026*	FILED
64/128,097	Publication-gap omnibus — quasineutral two-species expander DEC · provenance-gated / latency-split plasma control · as-built high-field winding & conductor architecture · *filed 7 Aug 2026, the evening before the arXiv drop*	FILED

TRADEMARK & ORIGIN

FTK-98801894	Kronos Fusion Energy — trademark application	FILED
KR-2022-*	Original provisional family (KR-2022-00001 … 00027) · *27 filings, 2022*	PRIORITY

The narrow, defensible magnet novelty — the specific conductor and the digital-twin winding optimisation, not high-field REBCO as a category — is the commercial core that can earn ahead of any Q > 1 milestone, with markets in fusion magnet supply, MRI/NMR, accelerators, and proton therapy. The claim is scoped honestly: the high field is a *system field* result, not a stand-alone-coil record; the small-bore plug coil is structurally infeasible as a bare winding but resolved by a stress-managed structural shield (feasible-pending-FEA); and the winding-tape experiment returned a *null result*. The value is the method, not a field record.

THE TEAM

Founding partners, board, advisors & auditors

Kronos is built by a bench of advanced-fuel-fusion, high-field-magnet, direct-conversion, and materials specialists, with a board and operations team drawn from defense, national laboratories, and industry. Dates are shown as ranges; where a tenure has ended or is term-ending, the range says so.

FOUNDING PARTNERS — SCIENCE

Dr. Gerald Kulcinski
Co-Founder · Helium-3 & Advanced-Fuel Fusion
UW–Madison · 2023–Present

Dr. Carl Weggel
Chief Scientist / S.M.A.R.T. Design
MIT Alcator Program · 2022–Present

Dr. Robert J. Weggel
Magnetic Field Design
MIT Magnet Lab · 2022–Present

BOARD

Priyanca Ford
Founder & CEO · Executive Board
2022–Present

Bandel Carano
Finance / Strategy
Oak Investment Partners / Stanford · 2025–2026

Patrick Schweiger
Fusion Device Engineering
Oklo / CFS / TerraPower · 2025–Present

SCIENTIFIC ADVISORS

Dr. Steven O. Dean
Fusion Policy & History
DOE / Fusion Power Associates · 2025–Present

Dr. Patrick H. Diamond
Plasma Turbulence & Transport
UC San Diego · 2025–Present

Dr. Jack J. Dongarra
HPC & Numerical Algorithms
Turing Award · 2025–Present

Dr. Nasr M. Ghoniem
Chief Material Scientist
UCLA · 2025–Present

Dr. Siegfried Glenzer
Plasma Physics & Laser Fusion
Stanford / SLAC · 2022–Present

Dr. David A. Hammer
Pulsed-Power Fusion
Cornell · 2025–Present

Dr. Donald A. Spong
Plasma Theory & Confinement
ORNL · 2025–Present

Dr. Curtis Smith
Risk Assessment & Nuclear PRA
MIT / Idaho National Lab · 2025–Present

RADM (Ret.) David Goggins
Naval Engineering & Power-Plant Design
U.S. Navy · 2023–2026

Dr. Konstantin Batygin
Mathematician
Caltech · 2022–2025

Dr. Ruben Fair
Magnet Design / ITER Liaison
PPPL / Jefferson Lab · 2022–2025

Dr. Paul S. Weiss
Materials & Nanotechnology
UCLA · 2022–2025

SCIENTIFIC AUDITORS

Dr. Wilfred A. Cooper
Plasma Equilibrium Theory
EPFL / Swiss Plasma Center · 2025–Present

Dr. Ahmed Hassanein
Plasma–Material Interactions
Purdue / Argonne · 2025–Present

Dr. Patrick E. Hopkins
Extreme Thermal Materials
U. of Virginia · 2025–Present

Dr. Peter Hosemann
Materials Joining & Structural Integrity
UC Berkeley · 2025–Present

Dr. Travis W. Knight
Advanced Nuclear Fuels & Systems
U. of South Carolina · 2025–Present

Dr. Philippe Lebrun
Cryogenics & Magnet Cooling
CERN · 2025–Present

Dr. Nitendra Singh
Nuclear Safety & Fuel Cycle
ITER · 2025–Present

Dr. Guido Van Oost
Magnetic Confinement & Fusion Systems
Ghent University · 2025–Present

Dr. Gary S. Was
Radiation Materials & Structural Integrity
U. of Michigan · 2025–Present

Dr. Ray Sedwick
Direct Energy Conversion
U. of Maryland · 2025

OPERATIONS

Michael Laughlin
Chief Operating Officer
2022–Present

Martin Owens
Chief Strategy Officer
LANL / GE Hitachi · 2022–Present

MG (Ret.) Paul Pardew
Chief Contracting Officer
Army Contracting Command · 2022–Present

David Beck
Fusion Commercialization
U.S. Space Force · 2024–Present

Sushma Bhatia
Environmental & Legislative
Google · 2022–Present

Michael De Frenza
Technology Licensing
2023–Present

MG (Ret.) Robin L. Fontes
Cybersecurity & Defense
Army Cyber Command · 2022–Present

Vijay Gehani
Supply Chain & Components
INOX India · 2024–Present

Jon Michel Greenwood
IT & AI Infrastructure
Live Nation · 2023–Present

Brian C. O'Neill
National Security
CIA / ODNI · 2022–Present

Gen. (Ret.) Gustave F. Perna
DoD Liaison
Operation Warp Speed · 2022–2023

Andrea Romero
Marketing Lead
2022–Present

Legal counsel is retained; those roles are held on the internal roster and are not listed here.

SOURCES

References

1 J E Menard *et al*, Fusion nuclear science facilities and pilot plants based on the spherical tokamak, *Nucl. Fusion* **56** 106023 (2016). doi:10.1088/0029-5515/56/10/106023

2 B N Sorbom *et al*, ARC: a compact, high-field, fusion nuclear science facility and demonstration power plant with demountable magnets, *Fusion Eng. Des.* **100** 378 (2015). doi:10.1016/j.fusengdes.2015.07.008

3 M E Austin *et al*, Achievement of reactor-relevant performance in negative triangularity shape in the DIII-D tokamak, *Phys. Rev. Lett.* **122** 115001 (2019). doi:10.1103/PhysRevLett.122.115001

4 A Marinoni, O Sauter and S Coda, A brief history of negative triangularity tokamak plasmas, *Rev. Mod. Plasma Phys.* **5** 6 (2021). doi:10.1007/s41614-021-00054-0

5 K Ioki *et al*, ITER vacuum vessel design and construction, *Fusion Eng. Des.* **87** 828 (2012). doi:10.1016/j.fusengdes.2012.02.023

6 T C Hender *et al*, Chapter 3: MHD stability, operational limits and disruptions, *Nucl. Fusion* **47** S128 (2007). doi:10.1088/0029-5515/47/6/S03

7 M Lehnen *et al*, Disruptions in ITER and strategies for their control and mitigation, *J. Nucl. Mater.* **463** 39 (2015). doi:10.1016/j.jnucmat.2014.10.075

8 A H Boozer, Theory of tokamak disruptions, *Phys. Plasmas* **19** 058101 (2012). doi:10.1063/1.3703327

9 S P Gerhardt, Dynamics of the disruption halo current toroidal asymmetry in NSTX, *Nucl. Fusion* **53** 023005 (2013). doi:10.1088/0029-5515/53/2/023005

10 C F Clauser, S C Jardin and N M Ferraro, Vertical forces during vertical displacement events in an ITER plasma and the role of halo currents, *Nucl. Fusion* **59** 126037 (2019). doi:10.1088/1741-4326/ab440a

11 A F Battey *et al*, Design of passive and structural conductors for tokamaks using thin-wall eddy current modeling, *Nucl. Fusion* **64** 016010 (2024). doi:10.1088/1741-4326/ad0bcf

12 A Zolfaghari, P Titus *et al*, Analysis of NSTX Upgrade OH magnet and center stack, *Fusion Sci. Technol.* **60** 736 (2011). doi:10.13182/FST11-A12459

13 K Ilin, K A Yagotintsev, C Zhou *et al*, Experiments and FE modeling of stress–strain state in ReBCO tape under tensile, torsional and transverse load, *Supercond. Sci. Technol.* **28** 055006 (2015). doi:10.1088/0953-2048/28/5/055006

14 S Hahn *et al*, 45.5-tesla direct-current magnetic field generated with a high-temperature superconducting magnet, *Nature* **570** 496 (2019). doi:10.1038/s41586-019-1293-1

15 S Hahn *et al*, No-insulation multi-width winding technique for high temperature superconducting magnet, *Appl. Phys. Lett.* **103** 173511 (2013). doi:10.1063/1.4826217

16 E L Wilson, A Der Kiureghian and E P Bayo, A replacement for the SRSS method in seismic analysis, *Earthquake Eng. Struct. Dyn.* **9** 187 (1981). doi:10.1002/eqe.4290090207

17 N M Newmark and W J Hall, *Earthquake Spectra and Design*, Earthquake Engineering Research Institute, Berkeley (1982).

18 A K Chopra, *Dynamics of Structures: Theory and Applications to Earthquake Engineering*, 5th edn, Pearson, Hoboken (2017).

19 P C Paris and F Erdogan, A critical analysis of crack propagation laws, *J. Basic Eng.* **85** 528 (1963). doi:10.1115/1.3656900

20 T L Anderson, *Fracture Mechanics: Fundamentals and Applications*, 4th edn, CRC Press, Boca Raton (2017).

21 S P Timoshenko and J N Goodier, *Theory of Elasticity*, 3rd edn, McGraw-Hill, New York (1970).

22 G Dhondt, *The Finite Element Method for Three-Dimensional Thermomechanical Applications*, Wiley, Chichester (2004). [CalculiX]

23 R Cimrman, V Lukes and E Rohan, Multiscale finite element calculations in Python using SfePy, *Adv. Comput. Math.* **45** 1897 (2019). doi:10.1007/s10444-019-09666-0

24 L L Lao, H St John, R D Stambaugh, A G Kellman and W Pfeiffer, Reconstruction of current profile parameters and plasma shapes in tokamaks, *Nucl. Fusion* **25** 1611 (1985). doi:10.1088/0029-5515/25/11/007

25 J Degrave *et al*, Magnetic control of tokamak plasmas through deep reinforcement learning, *Nature* **602** 414 (2022). doi:10.1038/s41586-021-04301-9

26 J Kates-Harbeck, A Svyatkovskiy and W Tang, Predicting disruptive instabilities in controlled fusion plasmas through deep learning, *Nature* **568** 526 (2019). doi:10.1038/s41586-019-1116-4

27 J P Freidberg, *Ideal Magnetohydrodynamics*, Plenum Press, New York (1987).

28 American Society of Civil Engineers, *Seismic Design Criteria for Structures, Systems, and Components in Nuclear Facilities*, ASCE/SEI 43-05, Reston, Virginia (2005).

29 A J Creely *et al*, Overview of the SPARC tokamak, *J. Plasma Phys.* **86** 865860502 (2020). doi:10.1017/S0022377820001257

30 P I Ford, *Kronos Physics De-Risking Register*, Kronos Fusion Energy 2026 series. doi:10.5281/zenodo.22133057

COLOPHON

How this document was made

The Kronos Fleet — Combined Editorial, 2026 is set in **Fraunces** (display), **Gelasio** (text), and **IBM Plex Mono** (data & equations), carried forward from the Kronos editorial design system.

The figures are rendered at 300 dpi from the deposited generator scripts; the document is composed as a single self-contained file with embedded fonts and imagery, paginated to US Letter, and rendered to PDF through a headless Chromium engine in matched light and dark editions.

Every headline quantity carries an evidence class; withdrawn and restated values are marked as such. Nothing herein is frozen beyond the founder-approved Tier-A set.

Explore it live — turn the interactive 3-D model, run the deposited solvers in the physics validator, and watch the companion film series.

LEGAL NOTICE

Notice, status, and distribution

Conceptual design & simulation study. This document reports a conceptual design and simulation study. It is not a construction commitment, a safety-analysis report, a regulatory filing, or an offer of securities. Forward-looking statements — schedules, costs, market sizes, and performance — are estimates subject to the limitations set out in the Simulations part and may change.

Numbers and their classes. Quantities are reported with evidence classes and case labels; modelled, assumed, and requirement-class values are identified as such and are not to be quoted without their labels.

Public edition. This edition carries the physics and design only; all financial, funding, and defense-commercial content has been removed for public distribution. The scientific text corresponds to the arXiv and journal submissions.

THE 2026 KRONOS SERIES

One programme, many papers

This editorial is one paper in the Kronos 2026 series — a real fusion company's complete, reproducible physics record for a spherical-tokamak breeder and its low-neutron D–^{3}He tandem-mirror burners. Every headline number is a frozen anchor in the Physics De-Risking Register.

Explore the whole programme: the De-Risking Register, the interactive 3-D model, and the physics validator.

KRONOS FUSION ENERGY

Vacuum-Vessel and Support Structural Mechanics Under Electromagnetic, Halo-Current, and Seismic Loads for a Compact Spherical-Tokamak Breeder

A real fusion company building real machines. Explore the science, live.

Zenodo · doi:10.5281/zenodo.22645838

Read on kronosfusionenergy.com

The Physics De-Risking Register